Heliyon 5 (2019) e01570

Contents lists available at ScienceDirect

Heliyon

www.elsevier.com/locate/heliyon

Influence of an applied current on the vortex matter in a superconducting sample with structural defects

C.A. Aguirre [a,*], Q.D. Martins [b], A.S. de Arruda [a], J. Barba-Ortega [c]

[a] Departamento de Física, Universidade Federal de Mato-Grosso, Cuiabá, Brazil
[b] Departamento de Física, Universidade Federal de Rondônia, Jí-Paraná, Brazil
[c] Departamento de Física, Universidad Nacional de Colombia, Bogotá, Colombia

ARTICLE INFO

Keywords:
Condensed matter physics
Electromagnetism

ABSTRACT

We show how the inclusion of a structural defect of determined geometry controls the vortex state in a square superconducting sample in the presence of an external magnetic field and a dc current. We simulated the defects by using the deformation parameter $\tau(x, y)$, solving the non-lineal time-dependent Ginzburg-Landau equations and using the link variable method, for four different geometries as possible options for the storage vortex, simulating the behavior of a capacitor. We found an exponential dependence of the current in which the first vortex penetrates the sample $\vec{J}_c$ as a function of the area of a square central defect in the sample. We also show the effect of the defects and the transport current on the magnetization, magnetic susceptibility, vorticity, and magnetic field at the first vortex entry into the sample H_1 and the density of the superconducting electrons.

1. Introduction

Currently the superconducting state is a powerful tool for applications in different and varied areas, such as medicine, technology, biotechnology, control and processing of data, material development, and field measurements, by means of slight interactions of the magnetic field [1,2,3,4,5,6,7]. This is due in large part to the main properties exhibited by different materials in the superconducting phase, such as current movement without Ohmnic losses, shielding of external fields, periodic oscillations in their susceptibility, and heat capacity, and over the last few years, control and movement of information through the manipulation of vortex cascades. This vortex manipulation in superconducting samples with different geometries and under different boundary conditions has been highly studied experimentally. One of the most successful investigations was carried out by A. V. Silhanek, where it was possible to guide a vortex current by positioning anti-dots in a sample with a specific geometry in the presence of an external current, with the added variation of the resistance in the sample as a voltage function [8]. Another result of importance was obtained by A. van Blaanderen et al.; they studied a sample with anti-pinnings and pinning centers and were able to steer the vortex movement along a defined path [9]. L. Van Look et al. studied the vortex pinning and the anisotropy in different samples, finding a dependence on the orientation of the electric field with respect to the critical current [10]. Also, D. Halbertal et al. conducted a study in which they performed magnetic measurements using SQUIDs and found variations in local temperatures in the samples [11]. K. J. Kihlstrom et al. found that mixed pinning landscapes in superconductors are emerging as an effective strategy for achieving high critical currents in high applied magnetic fields [12]. G. R. Berdiyorov et al. studied the static and dynamic properties of superconducting vortices in a superconducting stripe with a periodic array of normal metal regions in the presence of external electro-magnetic fields. They observed periodic entry and exit of vortices that reside in the metallic regions; also, the mobility of the weakly-pinned vortices can be reduced by increasing the magnetic field [13]. In several studies, the difference between the kinematic and the Abrikosov vortex and vortex-anti-vortex annihilation was shown [14,15,16,17,18,19,20,21]. In addition to the experimental papers, theoretical work has been carried out in which the resistance in a superconductor with an external current at zero magnetic field is studied, showing the variation of the resistance in the sample caused by the positioning of pinning-anti-pinnings centers and their modifications, and the stability of the various numerical methods used for these solutions [22,23,24,25,26,27]. Given the present importance that it represents for different applications, we present four different configurations of structural defects included in a superconducting nano-prism subjected to an external current and a magnetic field. We show how the vortex configuration can be steered by the geometry of the defect

* Corresponding author.
E-mail address: cristian@fisica.ufmt.br (C.A. Aguirre).

https://doi.org/10.1016/j.heliyon.2019.e01570
Received 30 November 2018; Received in revised form 23 February 2019; Accepted 23 March 2019

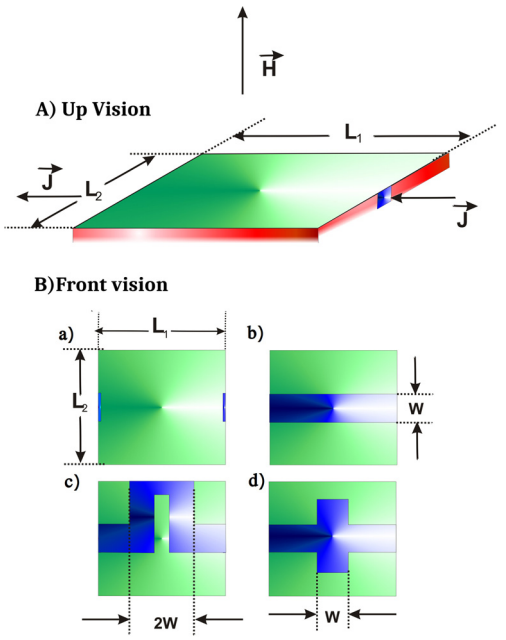

Fig. 1. Layout of the studied cases: $L_1 = 24\xi$, $L_2 = 16\xi$, $w = 4\xi$, for B-a) homogeneous sample with $\tau = 1.0$ in all green zones, except in the contacts (blue zone), B-b) Longitudinal section with area $A = L_1 w$, B-c) Non lineal section with area $A = 4w^2$, and B-d) Storage configuration. We take in all blue zones $\tau = 0.01$.

along a determined path. We present a form with this defect in order to establish a storage of the vortex in the superconducting sample. For all the cases studied, we show the magnetization M, magnetic susceptibility χ_m, vorticity N, and magnetic field that occurs with the first penetration vortex H_1 as a function of the magnetic field. This paper is organized as follows: In section 2, we introduce the theoretical formalism and all important variables. In section 3, the results obtained are described and discussed. Finally, in section 4, the conclusions are presented.

2. Theory

We consider a very thin square bridge of thickness $d \ll \xi$, so within this approximation we can neglect the demagnetization effects, and it can be treated as a two-dimensional problem [28]. The formalism used to study the system considered in Fig. 1(a-d) is given by the time-dependent Ginzburg-Landau (TDGL) equations [29,30,31,32,33]:

$$\frac{\mu}{\sqrt{1+\Gamma^2|\psi|^2}}\left[\frac{\partial\psi}{\partial t}+\frac{\Gamma^2\psi}{2}\frac{\partial|\psi|^2}{\partial t}+i\Phi\psi\right]-(-i\nabla-\mathbf{A})^2\psi + \psi(\tau(x,y)-|\psi|^2) \quad (1)$$

$$\frac{\partial\vec{A}}{\partial t} = \mathrm{Re}\left[\bar{\psi}(-i\nabla-\mathbf{A})\psi\right]-\kappa^2\left[\nabla\times\nabla\times\mathbf{A}\right] \quad (2)$$

In the equations (1) and (2), ψ represents the order parameter, A the potential vector, and $\kappa = 1.0$ is the Ginzburg-Landau parameter. The constants are taken to have the following values: $\Gamma = 10$ and $u = 5.75$, which are taken from the microscopic character of the superconductivity [33,34,35]. The equations are presented in adimensional form, as follows: $|\psi|$ in units of $\psi_\infty = \sqrt{-\alpha/\beta}$, lengths in units of the coherence length ξ, A in units of $H_{c2}\xi$, where H_{c2} is the second critical field, time in units of Ginzburg-Landau time $t_{GL} = \pi\hbar/8K_BT_c\eta$, scalar potential Φ in $\Phi_0 = \hbar/2et_{GL}$ units, and external applied current J in $J_0 = c\sigma\hbar/2et_{GL}$, where σ is the conductivity in the normal state. $dx = dy = 0.1\xi$ is the mesh sample. The usual superconducting-normal boundary conditions $(\nabla - i\vec{A})\psi\cdot n = 0$ are taken in non-contact sections, and in the contact sections we use the Dirichlet boundary condition $\psi_s = 0$. The TDGL equations must comply with the continuity equation $\nabla\cdot\vec{J} + \partial_t\rho(\vec{r},t)$ and external current $\nabla^2\Phi = \nabla\cdot\vec{J}_s$. For a homogeneous sample, we use $\tau(x,y) = 1.0$, and for each defect $\tau(x,y) = 0.01$. For the order parameter study, we will only consider values close to H_1 ($H > H_1 + \epsilon$, with $\epsilon = 0.001H_1$) taken as a constant, in order to account for the quasi-constant Lorentz force $\vec{F} = \vec{J}\times\vec{B}$, and this process will be followed for the configurations shown in Fig. 1(a-d) with $J = 0.0$ and $J_1 \sim J_c$ for each case.

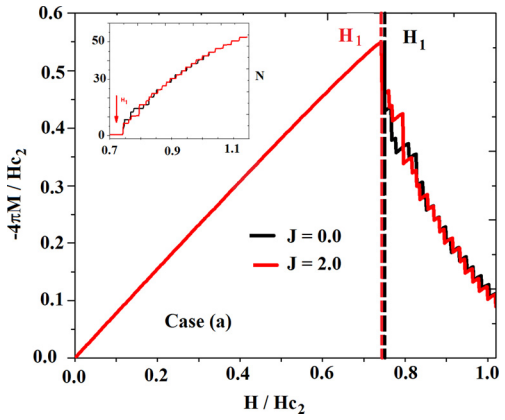

Fig. 2. Magnetization for the case (a). Inset vorticity as a magnetic field function $N(H)$.

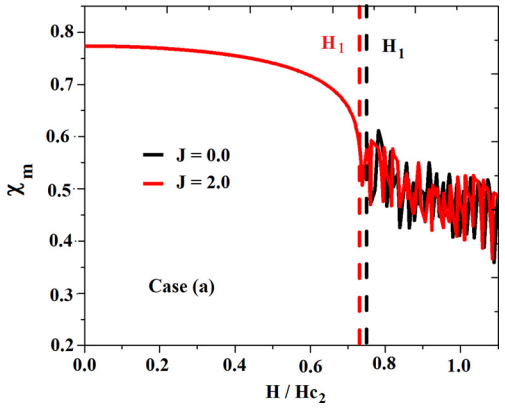

Fig. 3. Magnetic susceptibility, for the case(b).

3. Results and discussion

3.1. Case (a)

In Figs. 2 and 3, we show the magnetization (insets vorticity $N(H)$) and the magnetic susceptibility as functions of the magnetic field for case (a) for two values of the applied current: red line $J = 0.0$, black line $J = 2.0$. This shows that the system as usual exhibits the Meissner-Oschenfeld state for the $H \simeq 0.75$ fields, and we show H_1 in the figures. Since the change of the magnetization accounts for the entry of fluixoids in the sample but not for its possible movement in the sample, the variation of $\vec{J}$ to $\vec{J}_c$ does not appreciably change M, given the homogeneity of $\tau(x,y)$ in the sample. Therefore, in Fig. 4(a) we show ($\vec{J} = 0.0$), the Cooper pair density. In this figure, we show the entry of the vortex into the superconducting sample that is exhibited as a result of the depreciation of the superconductivity in the contacts and their respective movement to the central position and the equilibrium in the sample, given that they are Abrikosov vortices, after which the vortices are located at a distance for which there is a balance between the Lorentz force generated by the interaction between them and the effect that the depreciation of the superconductivity has on the points where the inclusion was generated from the contacts. It is thus shown that on making a

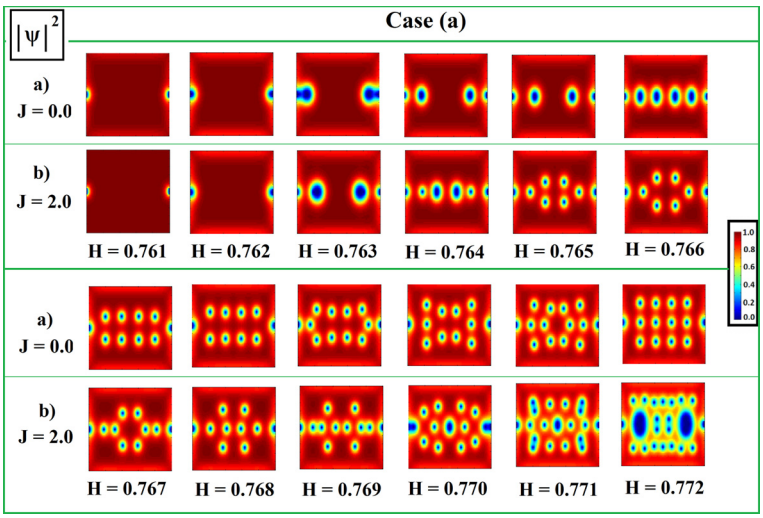

Fig. 4. Density of Cooper pairs at indicates H with a) $J = 0.0$ and b) $J = 2.0$, for the case (a).

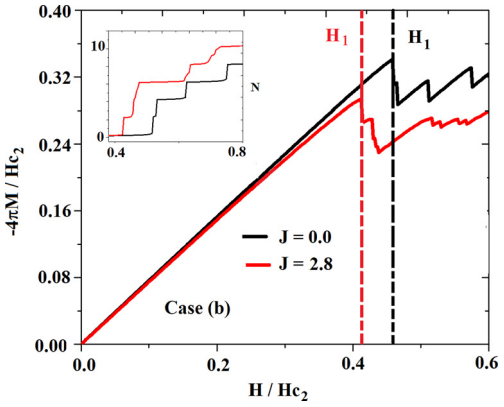

Fig. 5. Magnetization for the case (b). Inset vorticity $N(H)$.

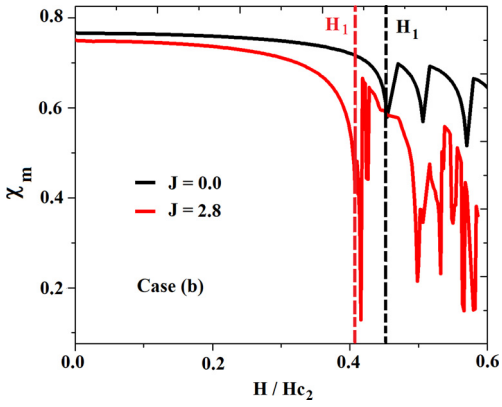

Fig. 6. Magnetic susceptibility, for the case (b).

small variation in the external field in the sample, there is a splitting of the vortex, and a movement perpendicular to the direction of the line that joins the contacts is generated, an expected effect as a function of that repulsion force. In Fig. 4(b), the vortex state is shown for the same H shown in Fig. 4(a). The difference lies in the inclusion of the external current $J = 2.0$, where the marked difference of the movement of that vortex and their interaction can be seen.

3.2. Case (b)

In Fig. 5, we can see that there is a decrease in H_1 compared to case (a) (Fig. 2), causing the vortex in the system to be created for smaller fields, and it is established that the critical current changes, an effect of exhibiting a value of $\tau(x, y)$ that is not homogenous in the sample. Additionally, the characteristic oscillatory behavior of the magnetic susceptibility can be seen as the vortex is created. Now in the case of the order parameter, the inclusion of the vortex is shown as the field is increased up to close to H_1, and as shown in Figs. 5 and 6, the vortex entry is in general periodical with an increase in this field, reaching a point of saturating the section in which $\tau(x, y)$ has been established on the surface of the superconductor, which would account for sections in which the order parameter would exhibit appreciable variations, more easily generating movement and interactions between phonons and superconducting electrons. It is important to observe the behavior of Figs. 7(a) and 7(b) and the differences in the order parameters, since both are for the same field values, but the inclusion of the current causes the vortex to enter more quickly into the region with $\tau(x, y) = 0.01$. Also, we show the difference in the values H_1 also observed for the two cases, an effect that is not appreciable in case (a) (Fig. 2).

3.3. Case (c)

In Figs. 8 and 9, we show the magnetization and magnetic susceptibility for case (c). As can be seen, the area of the defect is greater than in cases (a) and (b), and the critical current $\vec{J}_c$ necessary to perform the vortex mobilization must also be increased. Now for the vorticity $N(H)$ (inset), the almost continuous vortex entry of the first 6 vortices can be seen for the field $H \simeq 0.4$ in the case for which the current was included, there being a difference from the previous case. Also, given the inhomogeneity of $\tau(x, y)$ in the sample, the critical fields are different. Given this, it can be seen that for the susceptibility for the case with currents there is a behavior that is not as smooth as for the case of the absence of currents. This is due to a possible additional vortex vibration in their equilibrium position, due to the external current. As in all cases, we show the behavior of the order parameter for both cases, (Figs. 10(a) and 10(b)). In Fig. 10(a), the coordinating movement of the vortex can be seen; however, in Fig. 10(b), the inclusion of the current causes the saturation to be much faster than for the region with $\tau(x, y)$.

3.4. Case (d)

For case (d), a particular section was established for the defect geometry without a connection to the outside, in order to generate the vortex storage inside, simulating capacitor behavior. We can see that initially there is no change in the value of H_1 for the cases with and

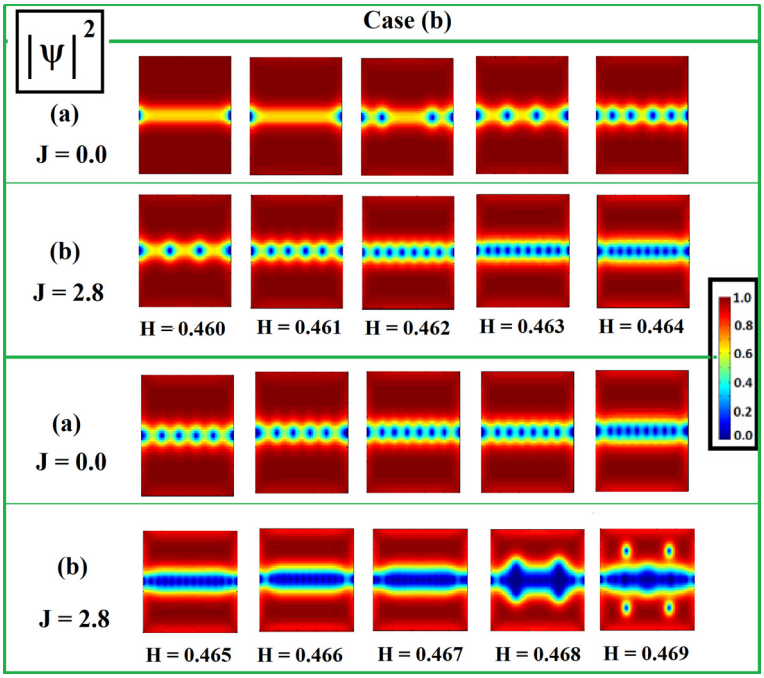

Fig. 7. Density of Cooper pairs at indicates H with a) $J = 0.0$ and b) $J = 2.8$, for the case (b).

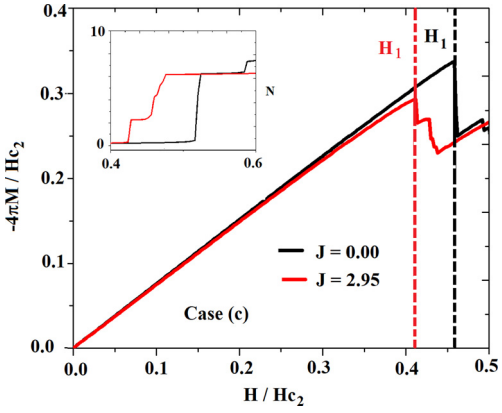

Fig. 8. Magnetization curves for the case (c).

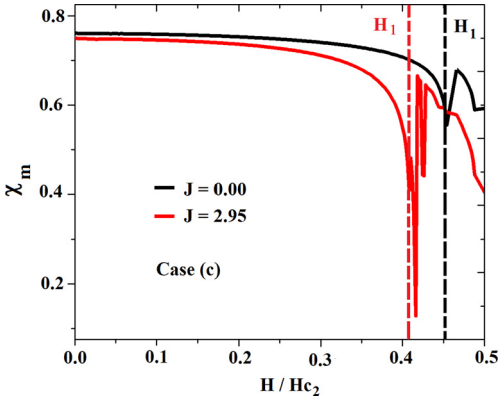

Fig. 9. Magnetic susceptibility for the case (c).

without current, because the effect of proximity is the same. Now in Figs. 11 and 12, it can be seen that for fields up to H_1, the values reached for the case with currents are greater. It is also shown that there is no decrease in $M(H)$ or $\chi_m(H)$, that is, the vortexes are stored directly in the sample, a behavior similar to that used in electromagnetism for the charges. In the case with currents, the magnetization is greater, and also the vorticity, i.e. more vortices are stored and with greater speed. This can be used in devices, according to the vortex current. However, there is a change in the case of the inclusion of currents, and it is due to the entry of the vortex outside the section established for their movement, because it exceeds the proximity energy barrier. In summary, in Table 1 we show the dependence of H_1, χ_m, and N on J for all the studied cases. It is always very interesting to look at the configuration of the vortex for the system in the presence and absence of an external current, (Fig. 13, establishing that the interaction between the external current and the pinning effect is very strong. In Fig. 14, we show a dependence of the critical current on the area of a square central defect of area A with $\tau(x, y) = 0.01$. The best theoretical fit was $J_c \simeq \exp(0.697 + 0.006A - 1.792A^2)$, showing an exponential growth of the critical current with the pinning center area. These results are very important from an experimental viewpoint.

Table 1
First vortex penetration field H_1, maximum of the magnetic susceptibility and vorticity for $J = 0$ and $J \neq 0$ conditions for all studied cases.

Case	H_1 for $J = 0$	H_1 for $J \neq 0$	χ_{max}	$N(H = 0.6)$
(a)	0.762	0.750	0.770	0 - 0
(b)	0.460	0.410	0.760	8 - 10
(c)	0.470	0.410	0.750	8 - 10
(d)	0.460	0.460	0.780	10 - 15

4. Conclusions

We have shown that with the aid of the deformation parameter $\tau(x, y)$ and an external current $\vec{J}$ applied in a mesoscopic superconducting square, there is an interesting pinning effect (vortex guide). It was shown that as $\tau(x, y)$ is included, there is a variation of the critical current in which the first vortex penetrates the sample $\vec{J}_c$. Also, we have shown the effect of the defects and the transport current on the magnetization, magnetic susceptibility, vorticity, and magnetic field at the first vortex entry into the sample H_1 and the density of the superconducting electrons. An analytical form of the critical current as a function of the area of the defect was found, $J_c \simeq \exp(0.697 + 0.006A - 1.792A^2)$.

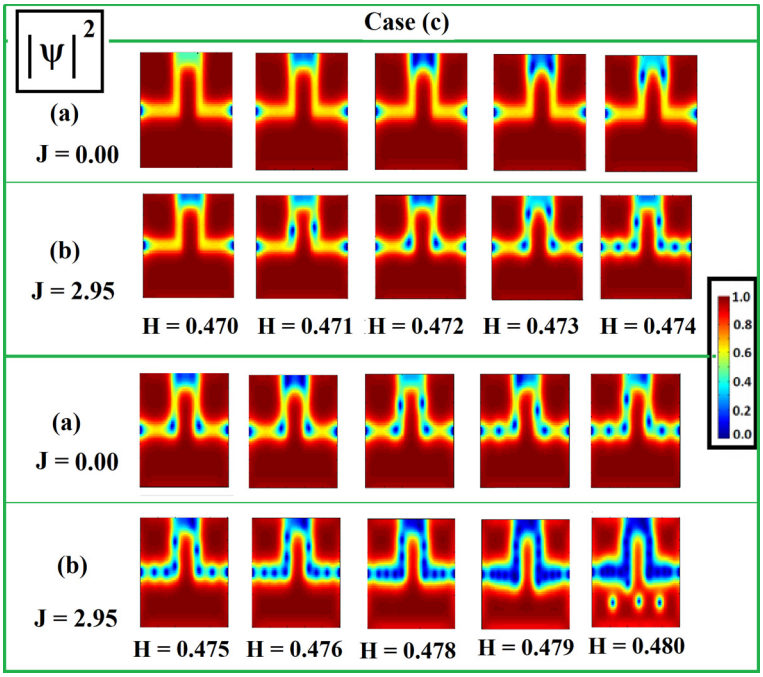

Fig. 10. Density of Cooper pairs at indicates H with a) $J = 0.0$ and b) $J = 2.95$, for the case (c).

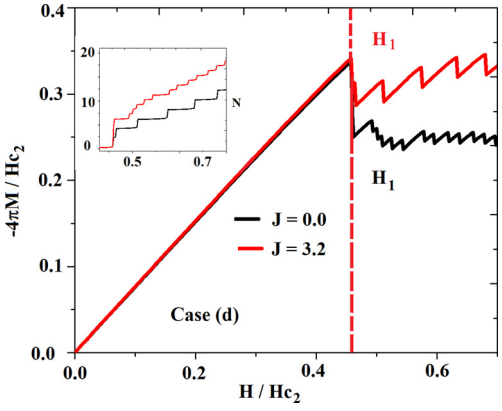

Fig. 11. Magnetization, for the system shown in Fig. 1(d).

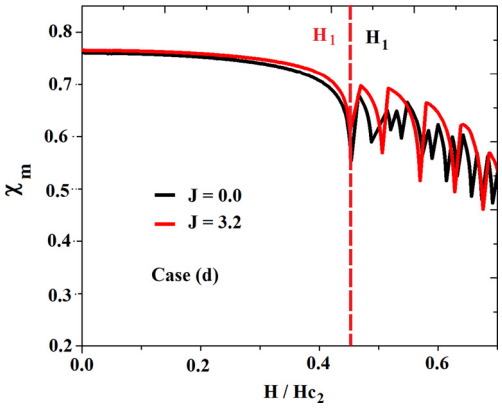

Fig. 12. Magnetic susceptibility, for the system shown in Fig. 1(d).

This result is very important from an experimental viewpoint, and it points to possible technological applications.

Declarations

Author contribution statement

C.A. Aguirre, Q.D. Martins, A.S. de Arruda, J. Barba-Ortega: Conceived and designed the analysis; Analyzed and interpreted the data; Contributed analysis tools or data; Wrote the paper.

Funding statement

C.A. Aguirre was supported by the Brazilian agency CAPES (089.229.701-89). Q.D. Martins was supported by the Brazilian agency CAPES.

Competing interest statement

The authors declare no conflict of interest.

Additional information

No additional information is available for this paper.

References

[1] J. Barba-Ortega, E. Sardella, J. Albino Aguiar, Superconducting boundary conditions for mesoscopic circular samples, Supercond. Sci. Technol. 24 (2011) 015001.
[2] C. Aguirre, M.R. Joya, J. Barba-Ortega, Effect of anti-dots on the magnetic susceptibility in a superconducting long prisma, J. Low Temp. Phys. 186 (2017) 250.
[3] P.G. de Gennes, J. Matricon, Collective modes of vortex lines in superconductors of the second kind, Rev. Mod. Phys. 36 (1964) 45.
[4] L. Komendova, M.V. Milošević, A.A. Shanenko, F.M. Peeters, Different length scales for order parameters in two-gap superconductors: extended Ginzburg-Landau theory, Phys. Rev. B 84 (2011) 064522.
[5] N.V. Orlova, A.A. Shanenko, M.V. Milošević, F.M. Peeters, A.V. Vagov, V.M. Axt, Ginzburg-Landau theory for multiband superconductors: microscopic derivation, Phys. Rev. B 87 (2013) 134510.
[6] J. Barba-Ortega, J.D. González, E. Sardella, Superconducting state of a disk with a pentagonal/hexagonal trench/barrier, J. Low Temp. Phys. 174 (2014) 96.
[7] B. Xu, M.V. Milošević, F.M. Peeters, Calorimetric properties of mesoscopic superconducting disks, rings, and cylinders, Phys. Rev. B 81 (2010) 064501.
[8] A.V. Silhanek, L. Van Look, S. Raedts, R. Jonckheere, V.V. Moshchalkov, Guided vortex motion in superconductors with a square antidot array, Phys. Rev. B 68 (2008).
[9] A. van Blaanderen, R. Ruel, P. Wiltzius, Template directed colloidal crystallization, Nature 385 (1997) 321.

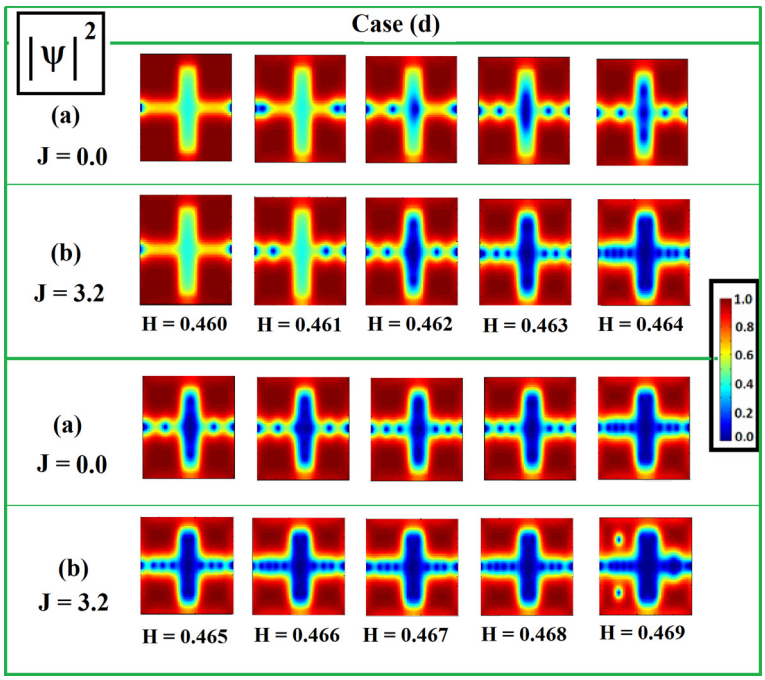

Fig. 13. Density of Cooper pairs at indicates H with a) $\vec{J} = 0.0$ and b) $\vec{J} = 3.2$, Fig. 1(d).

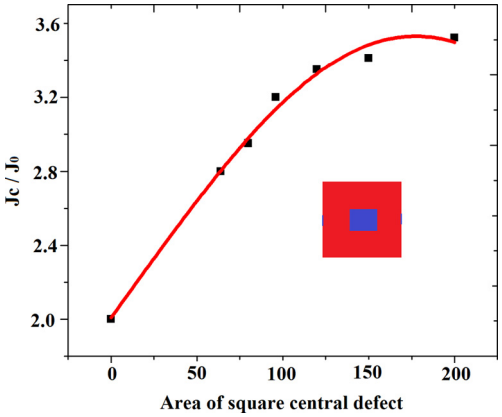

Fig. 14. Theoretical fitting for $\vec{J}_c$ for different areas of a central square defect of area A, $J_c = \exp(0.697 + 0.006A - 1.792A^2)$.

[10] L. Van Look, B.Y. Zhu, R. Jonckheere, B.R. Zhao, Z.X. Zhao, V.V. Moshchalkov, Anisotropic vortex pinning in superconductors with a square array of rectangular submicron holes, Phys. Rev. B 66 (2002) 214511.

[11] D. Halbertal, J. Cuppens, M. Ben Shalom, L. Embon, N. Shadmi, Y. Anahory, H.R. Naren, J. Sarkar, A. Uri, Y. Ronen, Y. Myasoedov, L.S. Levitov, E. Joselevich, A.K. Geim, E. Zeldov, Nanoscale thermal imaging of dissipation in quantum systems, Nature 539 (2016) 470.

[12] K.J. Kihlstrom, L. Fang, Y. Jia, B. Shen, A.E. Koshelev, U. Welp, G.W. Crabtree, W.K. Kwok, A. Kayani, S.F. Zhu, H.H. Wen, High field critical current enhancement by irradiation induced correlated and random defects in (Ba0.6K0.4)Fe2As2, Appl. Phys. Lett. 103 (2013) 202601.

[13] G.R. Berdiyorov, A.R. de C. Romaguera, M.V. Milošević, M.M. Doria, L. Covaci, F.M. Peeters, Dynamic and static phases of vortices under an applied drive in a superconducting stripe with an array of weak links, Eur. Phys. J. B 85 (2012) 13.

[14] J. Barba, E. Sardella, R. Zadorosny, Influence of the deGennes extrapolation parameter on the resistive state of a superconducting strip, Phys. Lett. A 382 (2018) 215.

[15] I.N. Askerzade, Numerical simulation of vortex nucleation in the two-band Ginzburg-Landau model, Tech. Phys. 55 (2010) 896.

[16] X. Wang, S.R. Ghorbani, S.I. Lee, S.X. Dou, C.T. Lin, T.H. Johansen, K.H. Müller, Z.X. Cheng, G. Peleckis, M. Shabazi, A.J. Qviller, V.V. Yurchenko, G.L. Sun, D.L. Sun, Very strong intrinsic flux pinning and vortex avalanches in (Ba,K)Fe2As2 superconducting single crystals, Phys. Rev. C 82 (2010) 024525.

[17] T. Golod, A. Rydh, V.M. Krasnov, Detection of the phase shift from a single Abrikosov vortex, Phys. Rev. Lett. 104 (2010) 227003.

[18] E.D. Gulian, G.G. Melkonyan, A.M. Gulian, Directed motion of vortices and annihilation of vortex/antivortex pairs in finite gap superconductors via hot-lattice, Phys. Lett. A 381 (2017) 2181.

[19] D. Castelvecchi, Quantum computers ready to leap out of the lab in 2017, Nature 541 (2017) 9.

[20] R. Zadorosny, E.C.S. Duarte, E. Sardella, W.A. Ortiz, Vortex/antivortex annihilation in mesoscopic superconductors with a central pinning center, Physica C 503 (2014) 94.

[21] G.R. Berdiyorov, A.D. Hernández-Nieves, M.V. Milošević, F.M. Peeters, D. Dominguez, Lux-quantum-discretized dynamics of magnetic flux entry, exit, and annihilation in current-driven mesoscopic type-I superconductor, Phys. Rev. B 85 (2012) 092502.

[22] Q. Du, Numerical approximations of the Ginzburg-Landau models for superconductivity, J. Math. Phys. 46 (2005) 095109.

[23] G.R. Berdiyorov, M.V. Milošević, F.M. Peeters, Kinematic vortex-antivortex lines in strongly driven superconducting stripe, Phys. Rev. B 79 (2009) 185506.

[24] G.R. Berdiyorov, M.V. Milošević, F.M. Peeters, Spatially dependent sensitivity of superconducting meanders as single-photon detectors, Appl. Phys. Lett. 100 (2012) 262603.

[25] M.P. Sørensen, N.F. Pedersen, M. Ögren, The dynamics of magnetic vortices in type II superconductors with pinning sites studied by the time dependent Ginzburg-Landau model, Physica C 533 (2017) 40.

[26] R. Wördenweber, E. Hollmann, J. Schubert, R. Kutzner, A.K. Ghosh, Vortex motion in high T_c films and a micropattern induced phase transition, Physica C 470 (2010) 835–839.

[27] C. Aguirre, H. Blas, J. Barba, Mesoscale vortex pinning landscapes in a two component superconductor, Physica C 558 (2018) 8.

[28] C.A. Aguirre, Q. Martins, J. Barba-Ortega, Analytical development of Ginzburg-Landau equations for superconducting thin film in presence of currents, UIS Ing. 18 (2) (2019) 213.

[29] R. Prozorov, Topology of the intermediate state in type I superconductors of different shapes, Phys. Lett. 98 (2007) 257001.

[30] M.A. Engbarth, S.J. Bending, M.V. Milošević, Geometry-driven vortex states in type-I superconducting Pb nanowires, Phys. Rev. B 83 (2011) 224504.

[31] J.R. Hoberg, R. Prozorov, Current-driven transformations of the intermediate-state patterns in type-I superconductors, Phys. Rev. B 78 (2011) 104511.

[32] G.R. Berdiyorov, B.J. Baelus, M.V. Milošević, F.M. Peeters, Stability and transition between vortex configurations in square mesoscopic samples with antidots, Phys. Rev. B 68 (4) (2003) 14205.

[33] J. Palacios, Metastability and paramagnetism in superconducting mesoscopic disks, Phys. Lett. 84 (2010) 1796.

[34] J.C. Pina, C.C. de Souza Silva, M.V. Milošević, Stability of fractional vortex states in a two-band mesoscopic superconductor, Phys. Rev. B 86 (2012) 024512.

[35] A.K. Elmurodov, F.M. Peeters, D.Y. Vodolazov, S. Michotte, S. Adam, F. de Menten de Horne, L. Piraux, D. Lucot, D. Mailly, Phase-slip phenomena in NbN superconducting nanowires with leads, Phys. Rev. B 78 (2008) 214519.